Microstructural Refinement in an Ultra-High Strength Martensitic Steel via Equal Channel Angular Pressing

S.L. Gibbons, R.A. Abrahams, M.W. Vaughan, R.E. Barber, R.C. Harris, R. Arroyave, I. Karaman

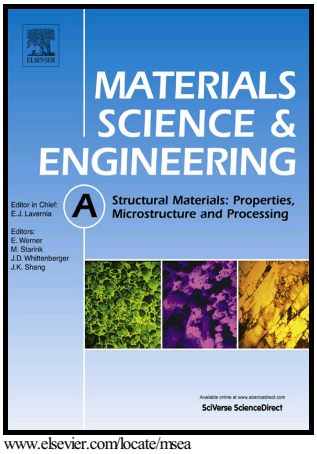

www.elsevier.com/locate/msea

PII: S0921-5093(18)30501-X
DOI: https://doi.org/10.1016/j.msea.2018.04.005
Reference: MSA36325

To appear in: *Materials Science & Engineering A*

Received date: 30 January 2018
Revised date: 29 March 2018
Accepted date: 3 April 2018

Cite this article as: S.L. Gibbons, R.A. Abrahams, M.W. Vaughan, R.E. Barber, R.C. Harris, R. Arroyave and I. Karaman, Microstructural Refinement in an Ultra-High Strength Martensitic Steel via Equal Channel Angular Pressing, *Materials Science & Engineering A,* https://doi.org/10.1016/j.msea.2018.04.005

Microstructural Refinement in an Ultra-High Strength Martensitic Steel via Equal Channel Angular Pressing

S.L. Gibbons[a*], R.A. Abrahams[a] , M.W. Vaughan[b], R.E. Barber[b], R.C. Harris[a] , R. Arroyave[b], I. Karaman[b]

[a]Air Force Research Laboratories/Munitions Directorate, Eglin AFB, FL, USA, 32542
[b]Department of Materials Science Engineering, Texas A&M University, TX, USA, 77843

[*]Corresponding author at: Air Force Research Laboratories/Munitions Directorate, Eglin AFB, FL, USA, 32542, USA. e-mail: sean.gibbons.5@us.af.mil

Abstract

In this work, a CALPHAD thermodynamic model is used to assess the thermodynamic stability of austenite in an Ultra-High Strength Martensitic Steel (i.e., Eglin Steel) in order to refine parent austenite-grain sizes, via high temperature equal-channel angular pressing (ECAP). The parent austenite-grain sizes are reduced from 188 μm to 14.8 μm, which in turn, led to the refinement of martensite lath sizes. This approach produced a yield strength of 1.68 GPa, ultimate strength of 1.98 GPa, and an elongation of 16.1%. Overall, this method reduced development cycle times and achieved alloy performance on par with Ni-Co secondary hardening steels.

Keywords: CALPHAD, Ultra-High Strength Steel, Equal Channel Angular Pressing, Grain Refinement, Martensitic Steel

1. Introduction

Ultra-High Strength Steels (UHSS) have garnered vast amounts of interest for their utility in mining [1] (e.g., drill bits, pipes, and structural materials), the automobile industry [2] (e.g., gears and frames), and in various aerospace applications [3] (e.g., landing gears). In particular, UHSSs offer enhanced strength (i.e., typically yield strengths, σ_Y, in excess of 1.38 GPa) with reasonable ductility (e.g., elongations at failure, ε_f, greater than 10%) [2]. Many alloys have been developed that meet these criteria [2], with some of the more common alloys being AerMet-100, HP-9-4-30, and AF1410, which require considerable amounts of alloying elements (see Table 1 for composition and typical properties) that can make widespread use cost prohibitive. As such, other high strength Ni-Cr-Mo martensitic alloys like 4335V have attracted significant interest, offering high performance with fewer elemental additions.

In the last decade, a new multicomponent Fe-Cr-Si-W-Mo UHSS developed by the U.S. Air Force Research Laboratory (AFRL) has emerged, also known as Eglin Steel (ES-1). ES-1 is a martensitic steel, which is strengthened by the semi-coherent precipitation of ε-carbide. The steel can achieve a 1.59 GPa minimum ultimate tensile strength, σ_{UTS}, and a 1.24 GPa minimum σ_Y through heat treatment alone, and it is also capable of achieving high low-temperature impact toughnesses (i.e., with more than 54 N-m of toughness at - 40˚C), which sets it apart from the aforementioned high strength martensitic alloys (e.g., 4335V). Despite the higher impact toughness and great hardenability of ES-1, its quasi-static tensile properties are only comparable to that of 4335V, falling short of the properties of the Ni-Co intermediate alloyed secondary hardening UHSSs, making ES-1 only practical for specific dynamic applications. As such, the desired goal is to reduce the performance gap between stage one tempering alloys in the class of ES-1 and the heavily alloyed Ni-Co secondary hardening UHSSs, while minimizing elemental additions.

Given the obvious difficulties in changing the composition of an alloy in order to improve performance, the clear choice is to enhance the properties through processing. Additionally, current conventional heat treatment procedures call for very high austenitizing temperatures (i.e., 1160˚C), which leads to undesirable grain growth and further reductions in properties (e.g., toughness [4] and σ_y [5]). There are many processing options available that can circumvent this issue and potentially increase the σ_{UTS} (e.g., via cold forming processes [6]), but the vast majority of them lead to an undesired reduction in cross sectional area and can significantly reduce the ductility, introduce anisotropy, and lead to cracking. In order to preserve initial material dimensions, Severe Plastic Deformation (SPD) methods were considered in this alloy development effort. Through SPD, high levels of strain can be introduced into the base material with little observed change in cross-sectional area [7]. In particular, Equal Channel Angular Pressing

(ECAP) was chosen for (i) its effectiveness in producing homogeneous ultra-fine grains by introducing vast amounts of strain while allowing the cross-sectional area to remain unchanged and (ii) for its potential to be upscaled.

ECAP has proven extremely successful in refining the microstructure in many steel alloys, such as interstitial free (IF) steels [8, 9], oxide dispersion strengthened (ODS) steels [10], and transformation induced plasticity (TRIP) steels [11, 12, 13]. However, there has been little success in using ECAP for grain refinement in UHSSs. Semiatin et.al. [14] demonstrated the susceptibility of a sub-critically annealed high strength Fe-Cr-Mo-Ni martensitic steel to shear localization during ECAP. Furthermore, the method, as described, is non-ideal for the processing of martensitic steels due to the reduced workability and tendency to reach the performance limits of the processing dies used. One method that can be used to overcome this limitation is to increase the processing temperature of the billets, which tends to make them easier to process [7] (e.g., due to the BCT to FCC transformation). Additionally, through proper thermodynamic assessment, temperatures can be chosen where favorable phase transformations occur that improve the ability of the material to flow. Unfortunately, grain sizes also increase with temperature and can lead to dynamic recrystallization [7], making it important to identify the lowest possible temperature at which the billets can be processed in the proper phase without reaching the load limit of the die.

As such, it would not be wise to ECAP ES-1 at room temperature due to the high strength martensitic structure. By elevating the temperature of ES-1 into the austenite phase region, the martensitic structure can be transformed back to austenite, creating a single phase FCC structure that is ductile enough to undergo ECAP. As demonstrated in this paper, the outlined method allows for the reduction in parent austenite grain sizes prior to transformation to martensite, which further constrains and reduces the size of the martensitic laths. This shows that through ECAP a nominal strength martensitic steel, such as ES-1, can achieve a σ_Y in excess of 1.38 GPa and a σ_{UTS} near 2.00 GPa. In the next section, the computational thermodynamic assessment of ES-1 as it pertains to the ECAP process is presented. The resulting analysis mapped regions of austenite stability that are key to developing the thermo-mechanical treatment (TMT) scheme for the present work. The following sections outline the derived TMT and the associated experimental procedures. The subsequent sections contrast the selected TMTs with their resulting properties and microstructure along with the associated conclusions.

2. Computational Thermodynamics

In order to process ES-1 using ECAP, the austenite phase stability must first be known. This could be done experimentally through the use of Differential Scanning Calorimetry (DSC) [15], which can require extensive experimentation. Computational methods can be used to quickly estimate the bounds of phase stability at equilibrium. Many thermodynamic phase assessment tools have been developed (e.g., ThermoCalc [16, 17], MTData [18, 19], PANDAT [20], FactSage [21, 22] and Gibbs and OpenCalphad [23, 24]) that are well suited for solving the thermodynamic states of a multi-component, multi-phase system given a set of thermodynamic conditions (e.g., overall composition, temperature, pressure). For the present study, ThermoCalc [16, 17] is used, utilizing the TCFE9 thermodynamic database, which is well defined for the compositional space of interest in this problem.

The assessment of the ES-1 system with respect to the variations in carbon (see the ES-1 phase diagram in Figure 1-a) showed that the system is prominently liquid above 1500˚C, with minor amounts of δ-ferrite forming below the liquidus temperature. The targeted austenitic region is found to be from 907˚C to 1415˚C at 0.29 wt.% C, with only minor amounts of M_6C and VC potentially forming just below this region down to 830˚C. Below 830˚C, ferrite becomes the dominant phase with various amounts of carbide phases. Because this is an equilibrium phase calculation, ThermoCalc does not take into account metastable phases and the observed sluggish kinetics inhibiting the formation of detrimental carbides (i.e., Fe_3C, $M_{23}C_6$, M_6C, and VC) as processing temperatures are reduced.

Given the calculated phase stability of ES-1 (see Figure 1-a), an optimal TMT strategy was constructed that consists of an optional subcritical anneal and three primary heat treatment stages (see Figure 1-b). The optional subcritical anneal (i.e., 677˚C ±10.0˚C for 10 hours with a furnace cool) is used to soften the bainitic matrix for machining, through the precipitation of spheroidized carbides that leads to the depletion of carbon. Stage 1 is a normalization step at 1163˚C ±10.0˚C for 4 hours followed by cooling in air, which is required since the thermal history of the material is often unknown and to ensure that all residual carbides are dissolved into solid solution prior to quenching and the formation of martensite. Stage 2 is the ECAP TMT step repeated twice, which involves heating the material to one of the two specified temperatures near the lower thermal boundary of the austenite phase region (i.e., 1050˚C ±10.0˚C and 950˚C ±10.0˚C) with a 0.5 hour hold time followed by ECAP and then water quench. The two temperatures were selected in the region of full austenitic thermodynamic stability well above the regions where $M_{23}C_6$, M_6C,

and VC can precipitate. Finally, Stage 3 consists of water quenching followed by tempering at 191˚C for 4 hours. This allows for the redistribution of carbon to dislocations and the subsequent precipitation of ε-carbide and age hardening of ES-1.

3. Experimental Setup

Consistent with the phase diagram in Figure 1-a, 10.16 cm diameter forged bars of Argon Oxygen Decarburized (AOD) and Vacuum Arc Remelted (VAR) ES-1 were sectioned into five 2.46 cm x 2.46 cm x 15.2 cm billets and subsequently heat treated using the strategy outlined in Figure 1-b. The billets were triple wrapped in 309 stainless steel foil and initially normalized at 1163˚C ±10.0˚C in a Thermo Scientific™ Lindberg/Blue M 1200˚C furnace for 4 hours followed by cooling in air. The three billets were then processed via the parameters in Table 2. The key factors considered when determining the suitability of ECAP for ES-1 were the die characteristics (i.e., angle and outer arc), crystallographic texture prior to pressing (i.e., near random orientation for prior austenite grains), and pressing speed and temperature [7]. As such, 2 of the billets were passed 2 times at a speed of 2.54 cm per second following Route C (i.e., 180˚ rotation along the long axis of the billet between each pass). The ECAP die used (see Figure 2-a) employed a two piece configuration with an upper and a lower die assembly that together created a 90˚ inner angle, φ, with a 0˚ outer arc of curvature, Ψ. The die was set to a temperature of 300˚C to mitigate surface cooling and thermal gradient induced stress cracking as much as possible. All of the samples processed experienced stress within acceptable limits (see Figure 2-b), with maximum loads of 1.05 GPa at 1050˚C ±10.0˚C and 1.26 GPa at 950˚C ±10.0˚C.

Samples for the electron backscattered diffraction (EBSD) were cut from near the center of the billets, perpendicular to the direction of flow, in order to assess grain refinement and orientation in fully processed regions. The samples were then mounted in Polyfast™ resin and mechanically polished with a vibratory polisher at the final step for 2 hours. EBSD images were acquired using a FEI Quanta 200FE scanning electron microscope with an EDAX EBSD detector. Hardness measurements (i.e., Rockwell C (HRC) and Microhardness (HV_{2000})) were also taken near the center of the billets, perpendicular to the direction of flow. Finally, cylindrical tensile samples (i.e., 0.318 cm gauge diameter and 1.27 cm gauge length) were machined from the billets, with the corresponding tensile axis parallel to the direction of flow. Tensile tests were conducted using an Instron 222 kN tensile tester at a strain rate of 2.33×10^{-4} per sec up to 0.699 mm of elongation (i.e., after onset of yielding) to identify σ_Y, then increased to 1.00×10^{-2} per sec until failure in accordance ASTM E8 to identify σ_{UTS}.

4. Results and Discussion

Analysis of the EBSD images at 2000x magnification (see Figure 3) showed significant reduction in prior austenite grain size with ECAP processing and the reduction in the processing temperature. Once the prior austenite grain boundaries were identified, a lineal intercept method was used to measure the average grain size. In the baseline sample (i.e., sample ES_{BL}), the prior austenite grains are easily observable with the average grain size of 188 µm ± 32.3 µm in diameter (ASTM grain size number 2), with highly textured packets of martensitic laths through the individual grains (see Figure 3-a). In the ECAP samples, resulting grain refinement made the direct assessment of prior austenite grain boundaries difficult, requiring a more rigorous comparison of martensitic lath orientations. By leveraging the Nishiyama-Wassermann orientation relationships for the martensitic transformation [25]:

$$\{111\}_\gamma // (011)_{\alpha'}; \langle \bar{1}01 \rangle_\gamma // \langle \bar{1}\bar{1}1 \rangle_{\alpha'} \qquad (1)$$

where there are 24 possible martensite variant orientations, an individual lath orientation can be isolated and other laths with the same semi-unique orientation can be mapped using EDAX OIM™ Data Analysis software [26]. By finding neighboring laths that share this symmetry relationship and are neighboring previously identified laths, the martensitic structures that resulted from the same prior austenite grain can be identified. Through this process the edges of the prior austenite domain can be mapped and their diameters can be quantitatively approximated.

With only 2 ECAP passes at 1050˚C ±10.0˚C (i.e., sample ES_{1050}), the average prior austenite grain size is reduced to 22.9 µm ± 9.60 µm in diameter (ASTM grain size number 8), with identifiable martensitic laths (see Figure 3-b). Additionally, 2 ECAP passes at 950˚C ±10.0˚C (i.e., sample ES_{950}), the average prior austenite grain size is further reduced to 14.8 µm ± 4.50 µm in diameter (ASTM grain size number 10) with now hard to distinguish martensitic laths (see Figure 3-c). Furthermore, the sizes of the individual laths were also directly measured using the EDAX Software [26] for comparison between the 3 cases (see Figure 3-d). By comparing the area fraction of binned lath diameters shown in Figure 3-d, it is clear that the martensitic lath structure is refined, as evident in the increase of area fraction in the bins near the 0.715 µm diameter lath size bin and the decrease in mean diameter (see Table 3) with decreasing ECAP temperature.

At 8000x magnification (see Figure 4), the reduction in martensitic lath sizes becomes more apparent (see Figure 4), with the largest laths being present in sample ES_{BL} (see Table 3). Sample ES_{1050} and ES_{950} exhibit similar mean lath diameters, with ES_{950} possessing a high concentration of laths below 1 μm. Another finding observed is an apparent bimodal distribution of grain sizes at 1050˚C and 950˚C. These images definitively show that the microstructure of ES-1 responded as expected to ECAP, reducing the prior austenite grain sizes prior to transformation to martensite, which in turn leads to the reduction of martensitic lath sizes.

Further analysis of the pole figure information at 2000x magnification (see Figure 5), reinforces the observations made about the prior austenite grain size distributions. Given the limited number of transformation orientations for martensite from an austenite grain, a larger number of prior austenite grains within the EBSD field of view would cause the pole figure densities to approach those of a randomly oriented sample. More specifically, maximum pole densities can be used to qualitatively assess their relative prior austenite grain sizes. As expected, non-random distribution of poles is greatest in sample ES_{BL} (see Figure 5-a), followed by ES_{1050} (see Figure 5-b) and then ES_{950} (see Figure 5-c), with maximum intensity values of 7.97, 2.55, and 2.35 respectively. This is in strong agreement with the assessment of the orientation relationships observed in the EBSD images (Figure and 4). These findings alone suggest that the sample ES_{950} would possess the greatest strength, since it possesses the smallest prior austenite grains and martensitic lath sizes, followed by samples ES_{1050} and ES_{BL}.

In addition to microscopy, all of the samples were mechanically tested for strength and hardness. The resulting engineering stress-strain data for the samples is plotted in Figure 6 and associated mechanical properties are listed in Table 4 and Table 5. As typical of ES-1, sample ES_{BL} exhibited a σ_Y of 1.36 GPa and a σ_{UTS} of 1.73 GPa with an ε_f of 11.9%, and HRC and HV_{2000} hardness values of 49.6 and 495, respectively. Further analysis of the ECAP tensile strengths showed that all of the samples now have σ_Y values greater than 1.38 GPa and the minimum attained σ_{UTS} of 1.84 GPa. The maximum values for σ_Y and σ_{UTS} were observed in sample ES_{950}, as 1.68 GPa and 1.98 GPa, respectively, where the ES_{950} process temperature was the lowest temperature in the fully austenitic region (see Figure 1-a) that resulted in a successful ECAP ausforming. Increases in elongation were observed, wherein ε_f increased with increasing temperature for 2 passes from 11.9% to 16.1%. Additionally, the uniform elongation, ε_u, decreased for ES_{950} (i.e., 3.60%), but increased for ES_{1050} (i.e., 4.10%) suggesting that the TMT routes can be tailored to control the ε_f. Furthermore, hardness increased for all of the ECAP samples with the highest values observed in sample ES_{950}.

With knowledge of the grain size distributions (i.e., prior austenite and martensitic laths) and mechanical properties, it becomes possible to assess the correlation between the two. The most common method for demonstrating this relationship is through the use of the Hall-Petch Equation:

$$\sigma_y = \sigma_i + \frac{k_d}{\sqrt{D}} \quad (2)$$

where σ_y is the yield stress, σ_i is the lattice friction factor, k_d is a constant, and D is the diameter of the associated grains or the microstructural length scale that dictates the dislocation mean free path [5, 27], which in this case the mean diameter was used. As such, the resulting mean grain sizes (i.e., austenite grain size and martensitic lath) and σ_y values were plotted and fit with first-order polynomials (see Figure 7) in order to determine σ_i and k_d. Assessment of the austenitic grains (see Figure 7-a) shows good linear agreement with Equation 2, exhibiting increased σ_y as grain sizes decrease, yielding a σ_i = 1.10 GPa and a k_d = 72.5 MPa-$mm^{1/2}$. Furthermore, the martensite lath size dependence of the yield strength also followed this relationship (see Figure 7-b), showing good linear agreement with Equation 2 (see Figure 7-b) with σ_i = 577 MPa and k_d = 56.6 MPa-$mm^{1/2}$.

The Hall-Petch relationship of the samples using the prior austenite grain size as well as the martensite length-scale work equally well. The strength in mar-tensite structures is controlled by the martensite mi-crostructural length-scales [28]. The fact that the Hall-Petch relationship works when considering the prior austenite grain can be explained by considering the effect that prior austenite grain has on the resulting martensite structure, since the martensite microstructural length-scale is indeed related to the prior austenite grain size. In fact, simplified geometric considerations have been used to connect the different length-scales across the martensite hierarchical microstructure to the prior austenite grain [28].

All of the attained results are consistent with what was expected from the ECAP of ES-1 except for the increase in elongation at failure. In many commonly ECAP processed materials, elongation initially decreases, then levels off [7] due to the heavily deformed microstructures and reduction in the dislocation storage capability upon subsequent strain path changes. This unexpected observation, opposite of what is expected, in the present work is attributed to the low number of ECAP passes utilized in this study which resulted in the bimodal distribution of grain sizes (see Figure 3-e and Figure 4-e) and led to the increase in elongation [29].

In this configuration, the prominently fine scaled grains that make up the matrix still enable the material to yield at greater strengths, while the larger grains allow for strain hardening mechanisms that stabilize tensile deformation [29]. Although the increase in ε_f was not initially postulated, the inhomogeneous microstructure is consistent with a

difficult to work material that has only under gone 2 ECAP passes. It is generally accepted that to achieve a homogeneous ultrafine grained microstructure using ECAP requires a minimum of four passes [7]. Furthermore, the reconfiguration of the microstructure through martensitic transformation in the heavily deformed austenite followed by the tempering should have contributed to the strain hardening capability of the samples and increased the elongation to failure.

With the increase in the ES-1 mechanical properties to σ_Y = 1.68 GPa, σ_{UTS} = 1.98 GPa, and the additional increase in elongation at failure, the position of ES-1 amongst other steels is greatly enhanced. Whereas standard heat treated VAR ES-1 mechanical properties are only marginally better than 4335V (i.e., 1.73 GPa and 11.9% elongation for ES-1 vs. 1.76 GPa and 8.00% elongation for 4335V), properties now meet or exceed several of the Ni-Co medium-alloy secondary hardening UHSS (e.g., HP-9-4-30, AF1410, and AerMet 100) (see Figure 8).

5. Summary and Conclusions

High temperature ECAP was shown to successfully refine the prior austenite grains and low temperature martensitic laths in ES-1, resulting in enhanced mechanical properties with respect to other steel alloys. More specifically, this study showed that:

1. Computational thermodynamics can be used in order to identify regions of austenite phase stability in ES-1 steels to successfully perform ECAP processing.

2. By heating ES-1 into the identified region of austenite stability all of the samples processed experienced loads within acceptable limits of the processing tool.

3. ECAP decreased prior austenitic grain sizes down to 15 µm and average martensitic lath sizes near 1 µm after only two passes at high temperatures.

4. ECAP in the austenite phase region led to an initial increase in tensile elongation at failure at room temperature to 16.1%, after ECAP at 1050˚C, from 11.9% of the baseline material, followed by a gradual decrease with lower ECAP temperatures.

5. With ECAP, a maximum σ_Y of 1.68 GPa and σ_{UTS} of 1.98 GPa were observed. This represents a significant improvement over the properties of 4335V steel. More importantly, the properties of ES-1 after ECAP can reach those of Ni-Co intermediate alloyed secondary hardening UHSSs, and with further process optimization have the potential to be increased more.

6. Future works should focus on varying the routes and the number passes to optimize grain refinement and to expand this method to similar alloy systems.

6. Acknowledgements

This research was funded under the U.S. Air Force Research Labs, the DoD SMART Program, the U.S. National Science Foundation, Division of Civil, Mechanical, and Manufacturing Innovation, Design of Engineering Materials Program under the grant number 1663130, and conducted in conjunction with Texas A&M University. The authors would also like to thank Dr. David Lambert for providing initial funding for these efforts through RW Chief Scientist Venture Funds Effort and the BLU-137 program for funding mechanical testing for test items.

7. Data availability

The raw/processed data required to reproduce these findings cannot be shared at this time due to technical or time limitations.

References

[1] C. Steel, "Wear & Impact Resistant Steel For The Mining Industry.," 4 Oct 2017. [Online]. Available: http://www.cliftonsteel.com/mining.html.
[2] T. J. Philip and T. V. McCaffrey, ASM Handbook, Volume 1: Properties and Selection: Irons, Steels, and High-Performance Alloys, vol. 1, ASM Handbook Committee, 1990, pp. 430-448.

[3] Y. Tomita, "Development of fracture toughness of ultrahigh strength low alloy steels for aircraft and aerospace applications," *Materials Science and Technology,* vol. 7, no. 6, pp. 481-489, 1991.
[4] S. Kim, S. Lee and B. S. Lee, "Effects of grain size on fracture toughness in transition temperature region of Mn--Mo--Ni low-alloy steels," *Materials Science and Engineering,* vol. A359, pp. 198-209, 2003.
[5] W. F. Smith, Structure and Properties of Engineering Alloys, New York: McGraw-Hill, 1993.
[6] G. E. Dieter and D. J. Bacon, Mechanical Metallurgy, New York: McGraw-Hill, 1986.
[7] R. Z. Valiev and T. G. Langdon, "Principles of equal-channel angular pressing as a processing tool for grain refinement," *Progress in Materials Science,* vol. 51, pp. 881-981, 2006.
[8] O. Saray, G. Purcek, I. Karaman, T. Neindorf and H. J. Maier, "Equal-channel angular sheet extrusion of interstitial-free (IF) steel: Microstructural evolution and mechanical properties," *Materials Science and Engineering A,* vol. 528, pp. 6573-6583, 2011.
[9] T. Neindorf, D. Canadinc, H. J. Maier and I. Karaman, "On the microstructural stability of ultrafine-grained interstitial-free steel under cyclic loading," *Metallurgical and Materials Transactions A,* vol. 38, pp. 1946-1955, 2007.
[10] M. Song, C. Sun, J. Jang, C. H. Han, T. K. Kim, K. T. Hartwig and X. Zhang, "Microstructure refinement and strengthening mechanisms of a 12Cr ODS steel processed by equal channel angular extrusion," *Journal of Alloys and Compounds,* vol. 577, pp. 247-256, 2013.
[11] S. Li, R. Zhu, I. Karaman and R. Arroyave, "Thermodynamic analysis of two-stage heat treatment in TRIP steels," *Acta Materialia,* vol. 60, pp. 6120-6130, 2012.
[12] S. Li, R. Zhu, I. Karaman and R. Arroyave, "Development of a kinetic model for bainitic isothermal transformation in transformation-induced plasticity steels," *Acta Materialia,* vol. 60, pp. 2884-2894, 2012.
[13] R. Zhu, S. Li, I. Karaman, R. Arroyave, T. Niendorf and H. J. Maier, "Multi-phase microstructure design of a low-alloy TRIP-assisted steel through a combined computational and experimental methodology," *Acta Materialia,* vol. 60, pp. 3022-3033, 2012.
[14] S. L. Semiatin and D. P. DeLo, "Equal channel angular extrusion of difficult-to-work alloys," *Materials and Design,* vol. 21, pp. 311-322, 2000.
[15] S. Raju, B. J. Ganesh, A. Banerjee and E. Mohandas, "Characterisation of thermal stability and phase transformation energetics in tempered 9Cr-1Mo steel using drop and differential scanning calorimetry," *Materials Science and Engineering,* vol. 465, pp. 29-37, 2007.
[16] J.-O. Andersson, T. Helander, L. Hoglund, P. Shi and B. Sundman, "Thermo-Calc and DICTRA, Computational tools for materials science," vol. 26, pp. 273-312, 2002.
[17] T.-C. Software, "Stockholm: Thermo-Calc Software," 4 Oct 2017. [Online]. Available: http://www.thermocalc.com/.
[18] R. H. Davies, A. T. Dinsdale, J. A. Gisby, J. A. J. Robinson and S. M. Martin, "MTDATA - Thermodynamics and Phase Equilibrium Software from the National Physical Laboratory," vol. 26, pp. 229-271, 2002.
[19] MTData, "Thermodynamics and Phase Equilibrium Software," 4 Oct 2017. [Online]. Available: http://www.npl.co.uk/science-technology/advanced-materials/mtdata/.
[20] S. L. Chen, S. Daniel, F. Zhang, Y. A. Chang, X. Y. Yan, F. Y. Xie, R. Schmid-Fetzer and W. A. Oates, "The PANDAT Software Package and its Applications," vol. 26, pp. 175-188, 2002.
[21] C. W. Bale, P. Chartrand, S. A. Degterov, G. Eriksson, K. Hack, R. B. Mahfoud, J. Melanon, A. D. Pelton and S. Petersen, "FactSage Thermochemical Software and Databases," vol. 26, pp. 189-228, 2002.
[22] T. GTT-Technologies, "FactSage 6.4," 4 Oct 2017. [Online]. Available: http://www.factsage.com/.
[23] R. E. Garcia, R. Arroyave, A. C. Powell and L. Li, "Gibbs - A Multi-Physics Thermodynamics Calculation and Visualization Suite," 4 Oct 2017. [Online]. Available: http://matforge.org/gibbs/.
[24] U. R. Kattner, B. Sundman, M. Palumbo and S. G. Fries, "Open Calphad - Software and Databases," Rio de Janeiro, Brazil, 2011.
[25] V. Yardley and E. Payton, "Austenite-martensite/bainite orientation relationship: characterisation parameters and their application," *Materials Science and Technology,* vol. 30, no. 9, pp. 1125-1130, 2014.
[26] E. S. Insight, "OIM Data Analysis Microstructure Analysis Software," 4 Oct 2017. [Online]. Available: http://www.edax.com/Products/EBSD/OIM-Data-Analysis-Microstructure-Analysis.aspx.
[27] I. Karaman, H. Sehitoglu, H. J. Maier, A. J. Beaudoin, Y. I. Chumlyakov and C. N. Tome, "Modeling of the Deformation Behavior of Hadfield Steel Single and Polycrystals due to Twining and Slip," *Acta Materialia,* vol. 48, p. 2031, 2000.
[28] E. I. Galindo-Nava and P. E. Rivera-Díaz-del-Castillo, "A model for the microstructure behaviour and strength evolution in lath martensite," *Acta Materialia* , vol. 98, pp. 81-93, 2015.
[29] Y. Wang, M. Chen, F. Zhou and E. Ma, "High tensile ductility in a nanostructured metal," *Nature,* vol. 419, pp. 912-915, 2002.

[30] C. T. Corporation, "Carpenter Technical Data Sheet: AerMet 100 Alloy," 4 Oct 2017. [Online]. Available: http://cartech.ides.com/.
[31] B. A. Becherer and T. J. Witheford, ASM Handbook, Volume 4: Heat Treating, vol. 4, ASM Handbook Committee, 1991, pp. 207-218.
[32] L. S. S. Company, "Product Data Sheets," 4 Oct 2017. [Online]. Available: http://customer.cartech.com/.

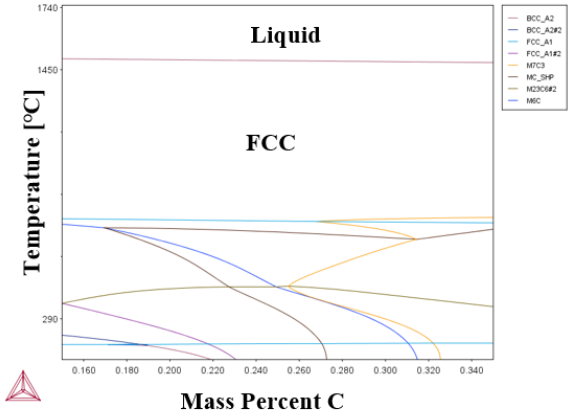

(a)

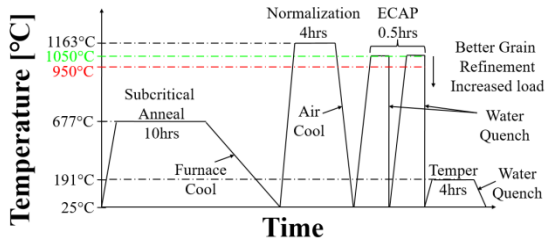

(b)

Figure 1: (a) The ThermoCalc derived phase diagram for ES-1 as a function of the wt.% of C and (b) the heat treatment strategy for the ECAP samples processed at two different temperatures: 1050˚C and 950˚C.

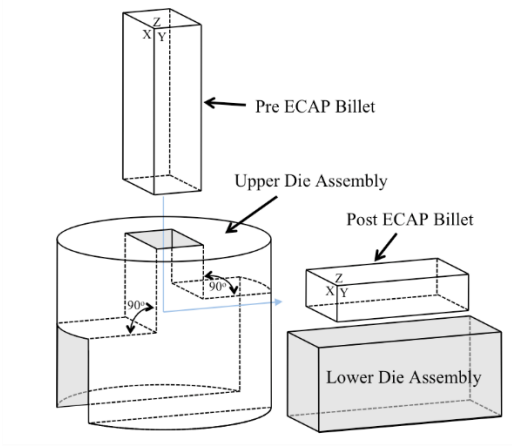

(a)

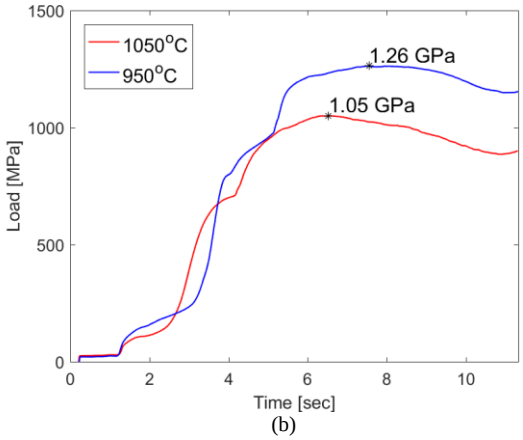

(b)

Figure 2: (a) Two piece ECAP die configuration with sharp 90° corner angles showing the botttom die slider concept that minimizes the friction during ECAP. (b) Associated stress data for ES-1 steel during first pass ECAP at two different temperatures.

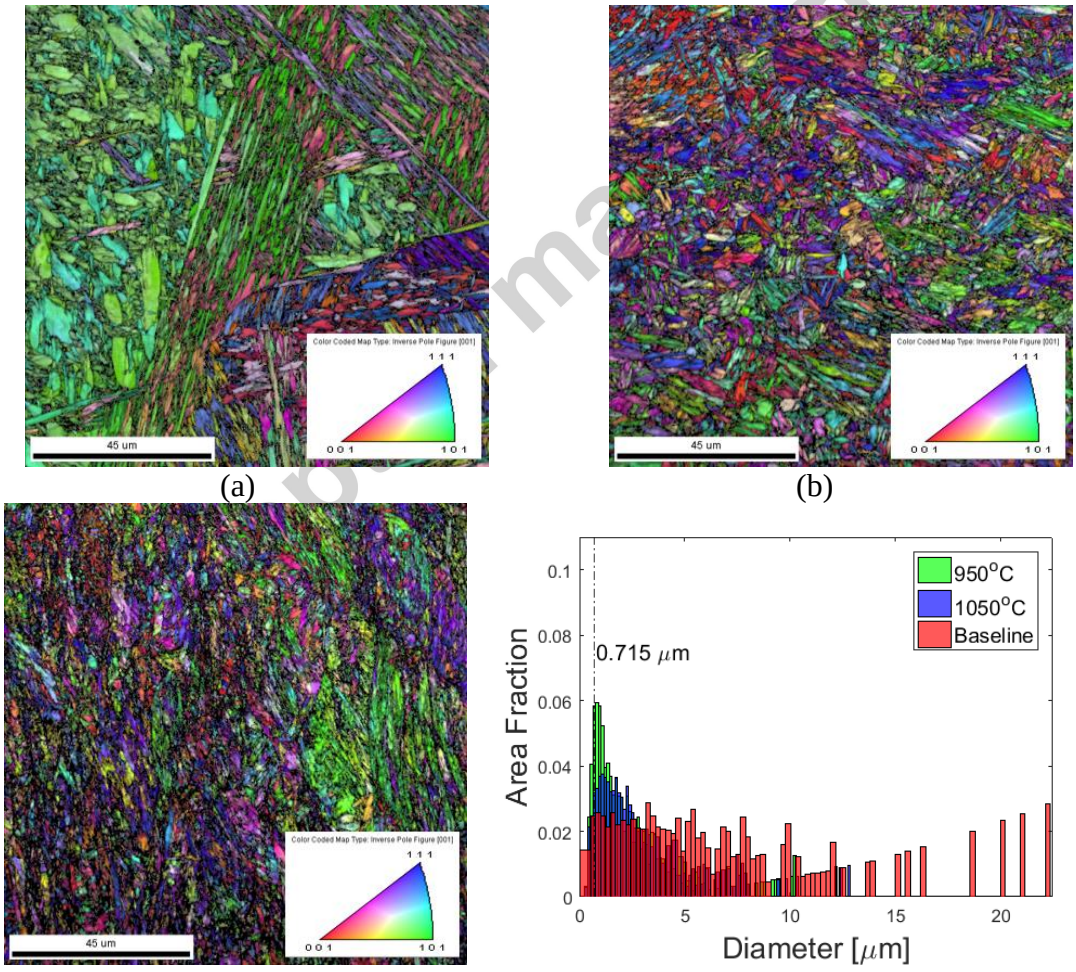

(a) (b) (c) (d)

Figure 3: EBSD images of martensitic lath orientation with color representing inverse pole figure [001] at 2000x resolution of ES-1 for samples (a) ES_{BL}, (b) ES_{1050}, and (c) ES_{950} in addition to (d) EBSD derived comparisons of area fractions versus grain diameter. BL: Baseline, ES_{1050}: ECAP sample processed at 1050 ℃, ES_{950}: ECAP sample processed at 950 ℃.

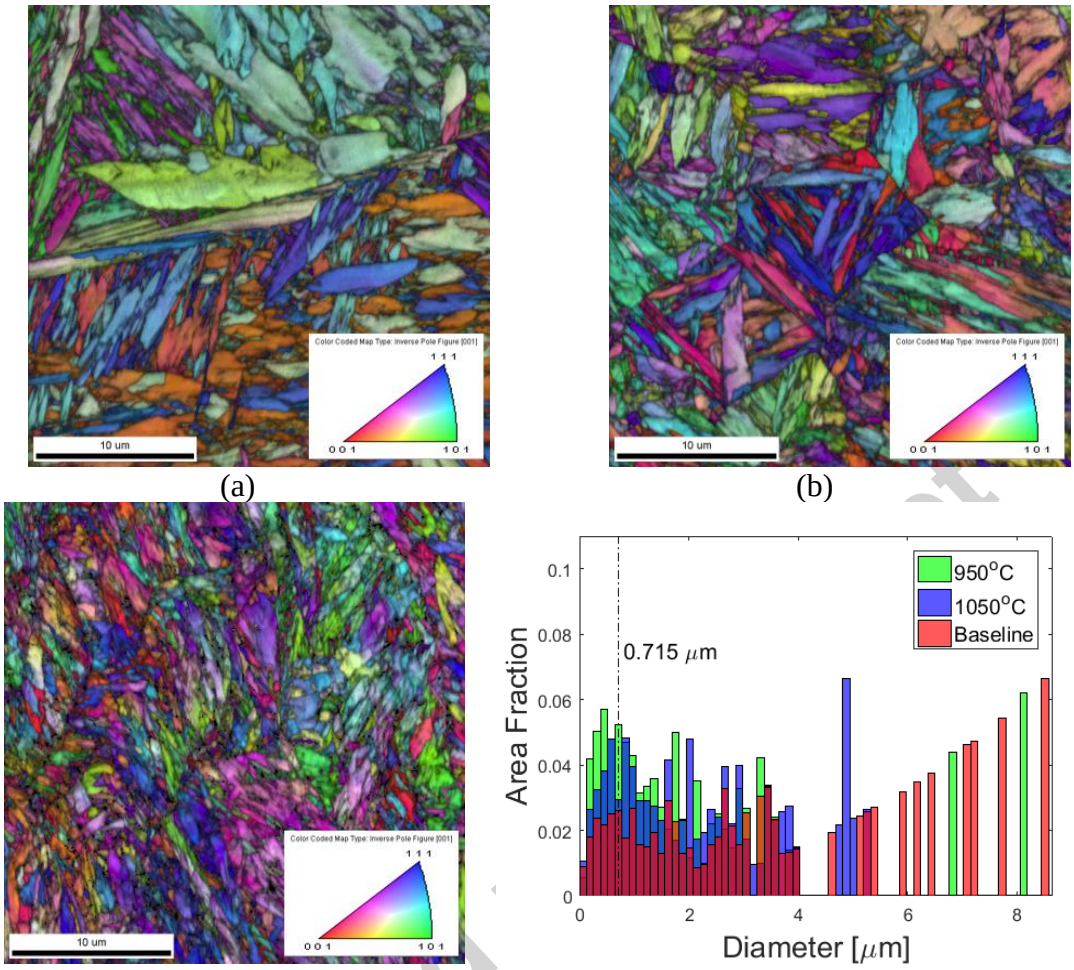

Figure 4: EBSD images of martensitic lath orientation with color representing inverse pole figure [001] at 8000x resolution of ES-1 for samples (a) ES_{BL}, (b) ES_{1050}, and (c) ES_{950} in addition to (d) EBSD derived comparisons of area fractions versus grain diameter.

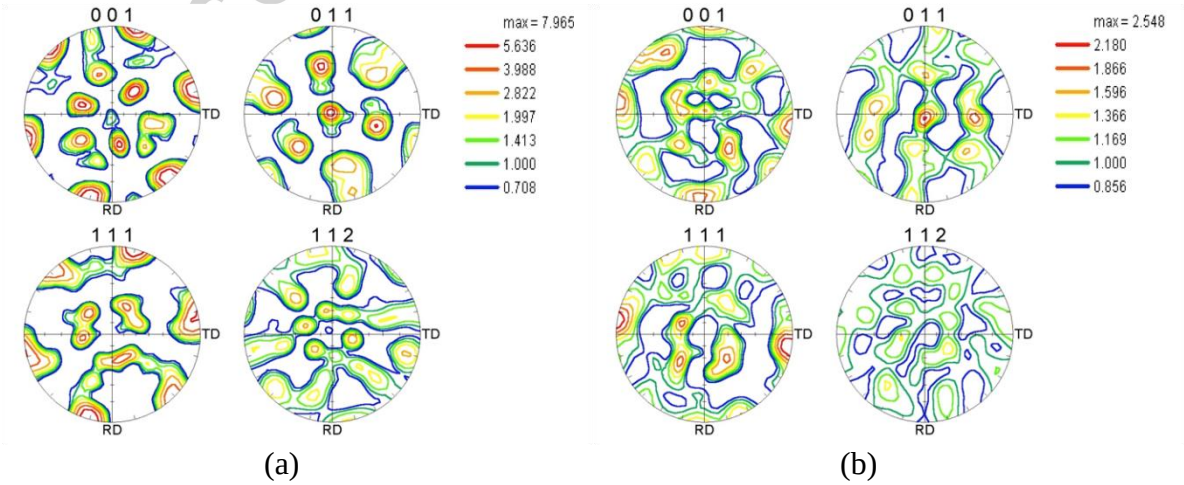

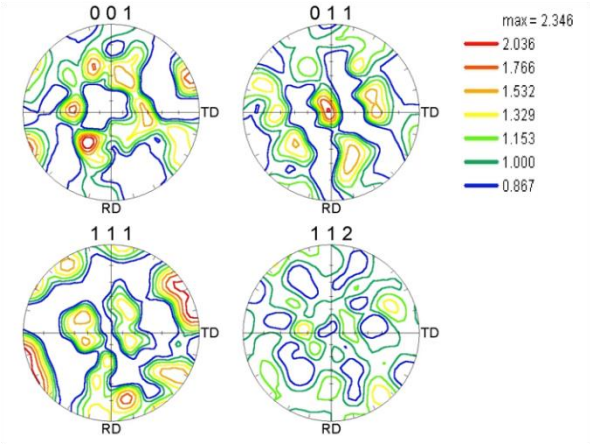

(c)

Figure 5: EBSD pole figures, at 2000x resolution, of ES-1 for samples (a) ES_{BL}, (b) ES_{1050}, and (c) ES_{950}.

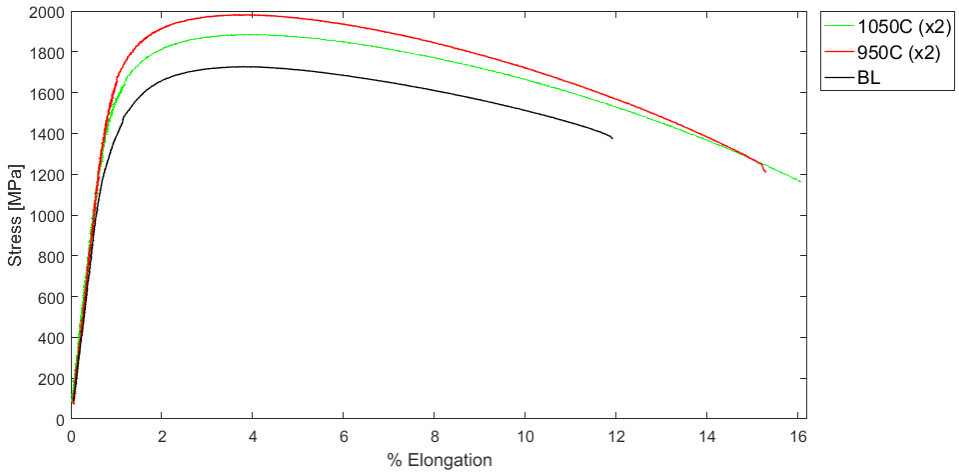

Figure 6: Room temperature engineering stress-strain responses of the samples ES_{BL}, ES_{1050}, and ES_{950}.

.

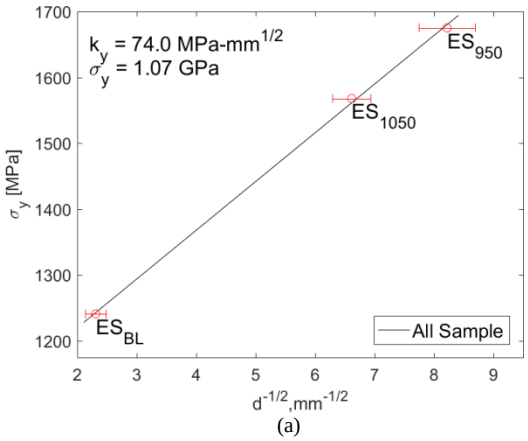

(a)

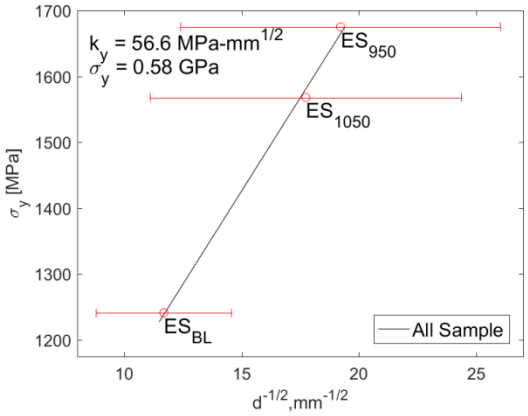

Figure 7: Grain size effects on σ_y as a function of (a) prior austenite grain size and (b) martensitic lath size.

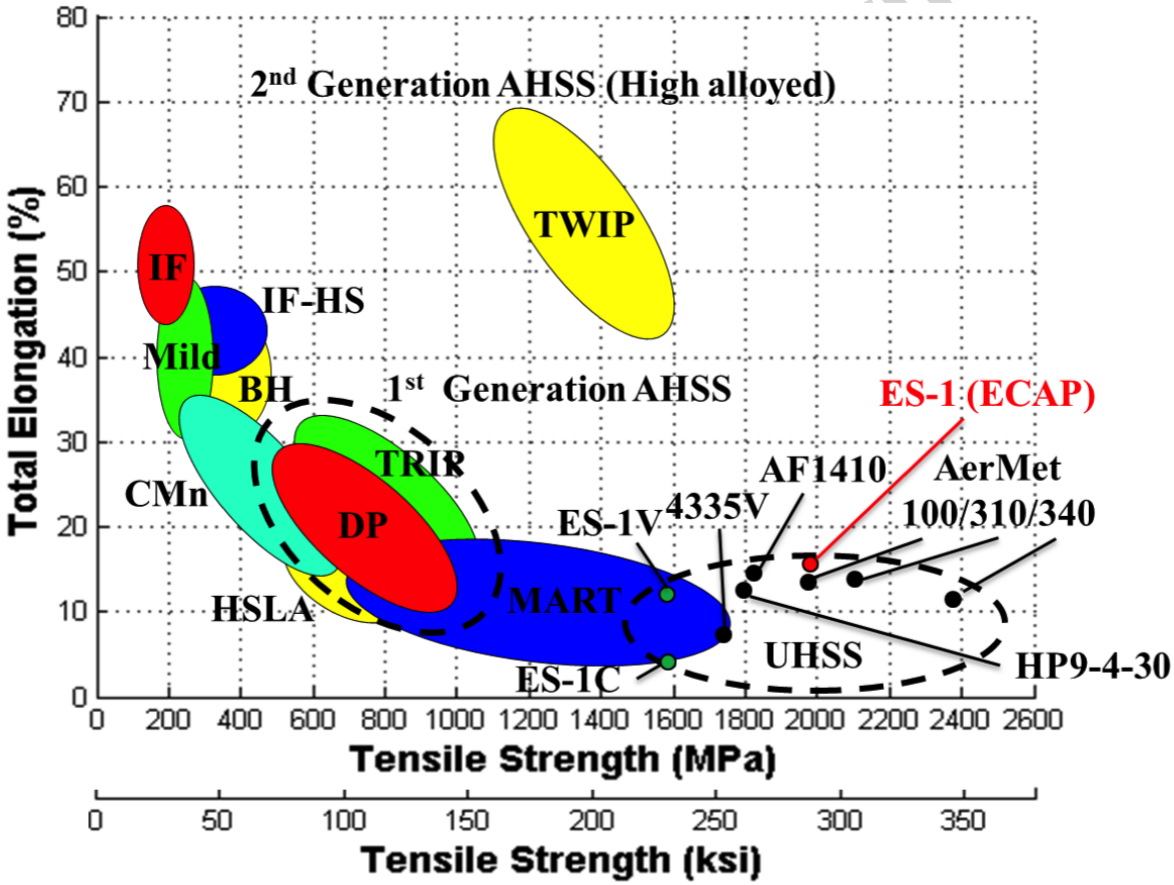

Figure 8: Typical mechanical properties for engineering steels where ES-1C represents Cast ES-1 without Hot Isostatic Pressing, ES-1V is VAR and forged ES-1, and ES-1 ECAP is ES-1 that has undergone ECAP in this study.

Table 1: Chemical composition of Ultra-High Strength Steel ES-1 (i.e., VAR and heat treated only) and common UHSSs along with typical values for Ultimate Tensile Strengths, UTS, and elongations at failure .

	Composition wt%:											
Elements	C	Si	Cr	Ni	Mo	Mn	V	W	Co	Fe	σ_{UTS} (GPa)	ε_f (%)
4335V	0.35	0.50	0.80	1.85	0.35	0.75	0.2	---	---	Bal	1.76	8.0
AerMet-100	0.23	---	3.10	11.1	1.20	---	---	---	13.4	Bal	1.97	14.0
HP-9-4-30	0.34	0.20	1.10	8.00	1.10	0.35	0.12	---	4.75	Bal	1.79	12.0
AF-1410	0.17	0.10	2.20	10.5	1.10	0.10	---	---	14.5	Bal	1.85	17.0
ES-1	0.29	1.10	2.85	1.10	0.50	0.70	0.10	1.10	---	Bal	1.59	13.0

Table 2: Processing conditions for the baseline (BL) sample and two billets processed via ECAP. The die temperature was 300℃.

Sample ID	# passes	Temp (˚C)	route	quench
ES_{BL}	0	---	---	---
ES_{1050}	2	(1050˚C)	C	water
ES_{950}	2	(950˚C)	C	water

Table 3: EBSD measured value of the martensite lath diameters with relative fraction of sub-micron measured at the 0.715 μm diameter and the mean grain size diameter showing the effect of ECAP on the martensite lath refinement.

	2000x	
Sample ID	0.715 μm bin size	mean dia (μm)
ES_{BL}	$2.58x10^{-2}$	7.32 ±5.86
ES_{1050}	$3.19x10^{-2}$	3.18 ±2.48
ES_{950}	$5.82x10^{-2}$	2.71 ±2.38
	8000x	
Sample ID	0.715 μm	mean dia (μm)
ES_{BL}	$2.60x10^{-2}$	3.96 ±2.63
ES_{1050}	$2.95x10^{-2}$	2.29 ±1.51
ES_{950}	$5.24x10^{-2}$	2.30 ±2.13

Table 4: Experimentally determined ES-1 mechanical properties from the uniaxial tensile tests performed along the long billet axis.

Sample	σ_Y (GPa)	σ_{UTS} (GPa)	ε_f (%)	ε_u (%)
ES_{BL}	1.36	1.73	11.9	3.80
ES_{1050}	1.51	1.84	16.1	4.10
ES_{950}	1.68	1.98	15.3	3.60

Table 5: Hardness values of process samples in HRC and HV. Errors are based on hardness readings from five points on a single sample.

Sample ID	HRC	HV_{2000}
ES_{BL}	49.5 ± 0.29	495 ± 11.9
ES_{1050}	50.4 ± 0.95	526 ± 4.70
ES_{950}	52.3 ± 0.22	578 ± 11.3